JACS
JOURNAL OF THE AMERICAN CHEMICAL SOCIETY

ARTICLE

pubs.acs.org/JACS

Charge Trapping and Storage by Composite P3HT/$PC_{60}BM$ Nanoparticles Investigated by Fluorescence-Voltage/Single Particle Spectroscopy

Zhongjian Hu and Andre J. Gesquiere*

NanoScience Technology Center, Department of Chemistry and CREOL, The College of Optics and Photonics, University of Central Florida, 12424 Research Parkway Suite 400, Orlando, Florida 32826, United States

Supporting Information

ABSTRACT: Fluorescence-voltage/single particle spectroscopy (F-V/SPS) was employed to study exciton−hole polaron interactions and interfacial charge transfer processes for pure poly(3-hexylthiophene) (P3HT) nanoparticles (NPs) and composite P3HT/$PC_{60}BM$ NPs in functioning hole-injection devices. F-V/SPS data collected on a particle-by-particle basis reveal an apparent bistability in the fluorescence-voltage modulation curves for composite NPs of P3HT and [6,6]-phenyl-C_{61}-butyric acid methyl ester ($PC_{60}BM$) that is absent for pure P3HT NPs. A pronounced deep trapping of free electrons photogenerated from the composite P3HT/$PC_{60}BM$ NPs at the NP/dielectric interface and hole trapping by fullerene anions in composite P3HT/$PC_{60}BM$ NPs under photoexcitation lies at the basis of this finding. The deep electron trapping effect reported here for composite conjugated polymer/fullerene NPs presents an opportunity for future application of these NPs in nanoscale memory and imaging devices.

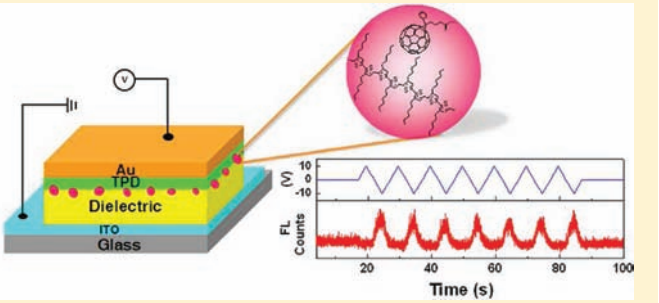

INTRODUCTION

Since the introduction of the conjugated polymer/fullerene bulk heterojunction (BHJ) concept over a decade ago,[1] the past decade has witnessed a burgeoning of research in the field of organic photovoltaics (OPVs).[2] The BHJ structure has also been employed as the active layer in *ambipolar* organic field effect transistors (OFETs) to provide both p- and n-channel functionality in the same device.[3] The primary photoexcitation in conjugated polymers is a Coulombically bound electron−hole pair (exciton) due to the low dielectric constant and significant electron−phonon interaction in organic materials.[4] When blended with electron acceptors such as fullerene, an ultrafast electron transfer process from the polymer (donor) to fullerene (acceptor) generates a charge transfer state (charge-transfer exciton), which can further dissociate into free charge carriers (hole and electron polarons) or recombine back to the ground state.[4,5] Considering the many excitations under optical stimulation, a situation arises where excitons and free carriers are present at the same time in the active layer of BHJ-based devices. Investigation of the optoelectronic processes and interactions involving these excitons and polarons are crucial, since they play a major role in determining device function and performance.[6] In addition, charge trapping due to extrinsic species, such as interface states and dopants, and intrinsic species, such as aggregates and excimers, is an important consideration as well.[7] Hence, investigation of the interactions between polarons and excited states as well as the charge trapping at interfaces within the BHJ structure and between the BHJ structure and other device layers (i.e., materials) present in a functioning device is of great significance.[8] However, the coexistence of excitons, polarons, charge-transfer states, as well as other chemical intermediates, in combination with the nanostructured complexity and heterogeneity of conjugated polymer bulk films, hampers the development of an in-depth understanding of how the coexistence and interactions between these species affect device function. Single molecule and single nanoparticle spectroscopy methods have been effective tools in removing complications caused by the study of bulk materials.[9] In particular, fluorescence-voltage/single molecule spectroscopy and fluorescence-voltage/single particle spectroscopy (F-V/SMS and F-V/SPS) have proven to be very useful tools in revealing the nature of intermediate states associated with fluorescence blinking, and the interactions between excitons and polarons. Specifically, singlet and triplet exciton quenching by hole polarons in single conjugated polymer molecules and nanoparticles,[10−14] and quenching of singlet excitons by triplets have been investigated.[15] Light-assisted hole injection from hole-transporting layers into single conjugated polymer chains has recently been reported.[16] F-V/SMS and F-V/SPS involve recording single molecule/nanoparticle fluorescence intensity transients while applying a triangular bias modulation on a device. These devices are basically hole-only capacitor devices or functioning diodes,[14,17] where the applied bias controls hole injection and removal kinetics

Received: August 2, 2011
Published: November 01, 2011

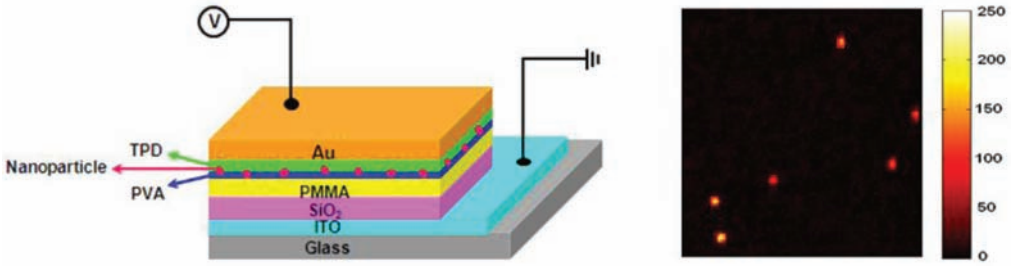

Figure 1. Device structure of a nanoparticle based hole-only capacitor device (left) and laser confocal scanning image (right, $10 \times 10\ \mu m^2$) of 50 wt % $PC_{60}BM$ blended P3HT NPs in a hole-only capacitor device at zero bias collected under 488 nm excitation from an Ar^+ laser with a power of 7.2 W/cm^2. The scale bar indicates counts per 5 ms.

at the interface of a hole transporting layer (HTL) and the single molecules/nanoparticles.

Herein, the F-V/SPS technique was applied to the study of pure and 50 wt % $PC_{60}BM$ blended P3HT NPs embedded in hole-only capacitor devices. The F-V/SPS technique was specifically applied to investigate the interaction between photogenerated excitons, photogenerated holes and electrons (free charge carriers through charge transfer from P3HT to $PC_{60}BM$), and injected holes (through applied bias) on a particle-by-particle basis for both pure P3HT NPs and composite P3HT/$PC_{60}BM$ NPs. In addition, charge trapping at the HTL/NP interfaces as well as the NP/dielectric interfaces was investigated. The devices were built on top of optically transparent ITO−glass substrates coated with dielectric layers on which the polymer NPs were deposited by spin coating. The devices were then finished by thermal deposition of *N,N′*-bis(3-methylphenyl)-*N,N′*-diphenylbenzidine (TPD) as a hole transporting layer that forms an electrical contact between the NPs and the gold top electrode. The device is schematically represented in Figure 1. In the case of these hole-only capacitor devices, with the molecules or NPs located at the dielectric interface, the fluorescence of these nanomaterials actually reports on the charging and discharging of the NPs and the NP/dielectric interface. When the hole concentration in the NPs and at the NP/dielectric interface is high, the fluorescence signal will be strongly quenched (forward bias operation, i.e. accumulation mode, or zero bias in the case of the composite NPs) while for vanishing hole concentrations the fluorescence signal will be unquenched (reverse bias operation, i.e. depletion mode). As such, the fluorescence-voltage signal can be interpreted as an optical derivative of a capacitance−voltage measurement, as will also be shown in the data presented herein. The distinction between pure P3HT and composite P3HT/$PC_{60}BM$ NPs is imperative here, since the composite P3HT/$PC_{60}BM$ NPs enable the continuous photogeneration of holes and electrons even under depletion mode.

The F-V/SPS data reported in this paper show that (i) 84% of pure P3HT NPs exhibit injected-hole-induced quenching of P3HT fluorescence due to energy transfer to holes present at the TPD/P3HT interface[12,14,18] and/or hole injection into the P3HT NPs,[12,14,16,18−21] (ii) quenching of P3HT emission in nearly all of the 50 wt % $PC_{60}BM$ blended P3HT NPs can be eliminated under negative bias (hole depletion), as observed by P3HT fluorescence recovery, indicating removal of holes on the polymer backbone before exciton quenching can occur, (iii) F-V/SPS data for all pure P3HT NPs and 50 wt % $PC_{60}BM$ blended P3HT NPs exhibiting low modulation depth do not show hysteresis, while (iv) almost all of the 50 wt % $PC_{60}BM$ blended P3HT NPs exhibiting moderate to high modulation depth do show hysteresis in the fluorescence-voltage sweeps. The variability in modulation depths for observations i, ii, and iii indicates that there are highly complex and heterogeneous energy and hole transfer processes occurring at the TPD/NP and NP/dielectric interfaces. The lack of hysteresis indicates that hole movement during hole sweep-in and sweep-out under bias is sufficiently fast and is not hampered by, for example, deep hole trapping. These observations are similar to those for previously studied poly[2-methoxy-5-(2′-ethyl-hexyloxy)-1,4-phenylene vinylene] (MEH-PPV) NPs and MEH-PPV single molecules.[13,14,19] However, in the presence of $PC_{60}BM$ (i.e., composite P3HT/$PC_{60}BM$ NPs), the fluorescence-voltage modulation data for single NPs clearly shows a strong hysteresis that can be attributed to significant electron trapping at the NP/dielectric interfaces. These data show that efficient photogeneration of free charge carriers in the composite P3HT/$PC_{60}BM$ NPs under illumination can actually lead to a build-up of interfacial charge (with associated interfacial dipoles) that not only strongly affects the interfacial charge transfer process at the nanometer scale but also leads to a charge-storage behavior. Our results correspond well with the memory functions (via optical programming and electrical erasing) demonstrated in bulk P3HT/$PC_{60}BM$ and P3HT/CdSe based OFET devices, which are caused by an electron trapping−detrapping mechanism.[22,23] The interfacial charge trapping also suggests possible applications in optical sensing and charge coupled devices (CCD).[24,25] Thus, the charge-storage effect reported here presents an opportunity for future exploration of conjugated polymer/fullerene NP applications in nanoscale memory and imaging devices.

EXPERIMENTAL SECTION

The conjugated polymer/fullerene composite NPs were fabricated by a reprecipitation method as reported in our previous work.[26] The hole−injection device was assembled bottom up with a metal−insulator−semiconductor geometry as shown in Figure 1. The multilayer device was fabricated on top of a commercially available patterned indium tin oxide (ITO) coverslip (Evaporated Coating, Inc., 50 Ω/□). A 200 nm thick SiO_2 insulating layer (ACI Alloys) was deposited through an e-beam evaporation system (Therminoics) followed by spin coating of a 100 nm poly(methyl methacrylate) (PMMA, Sigma Aldrich) layer from toluene. The PMMA layer helps to isolate the NPs from the SiO_2 layer and improve the NP photostability.[14] On top of the PMMA, a thin layer of 10−20 nm of polyvinyl alcohol (PVA) was spin coated from a water solution to make a hydrophilic surface favorable for further spin coating of an aqueous NP suspension. This assembly, to a large extent, ensures a close contact between the NPs and the hole-transporting layer. After the spin coating of the NPs suspensions, the device was transferred into a N_2 filled glovebox and dried in a N_2 atmosphere for 2 days. The

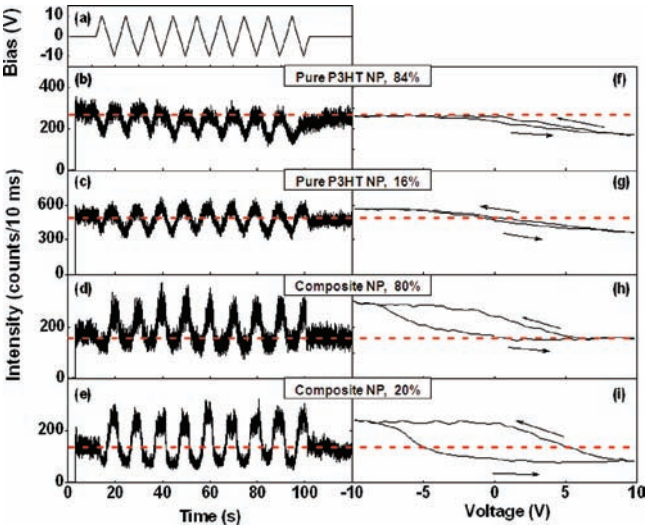

Figure 2. Typical fluorescence transient modulations (dwell time: 10 ms) of the representative majority of the (b) pure and (d) 50 wt % $PC_{60}BM$ blended P3HT NPs while repeatedly applying a triangle bias sequence (a) at a sweep rate of 4.0 V/s to the device in 12−102 s. Panels c and e present the modulation of a minority of pure and 50 wt % $PC_{60}BM$ blended NPs that show both fluorescence quenching at positive bias and recovery at negative bias, respectively. The type and percentage of NPs displaying different modulation behavior are shown as an inset. Panels f−i depict corresponding time averaged fluorescence modulation plots as a function of applied bias voltage for the transients shown in panels b−e. The arrows in panels f−i signify the direction of the bias scan. The corresponding fluorescence modulation characteristics at a higher sweep rate of 40 V/s collected for the same NPs are given in Figure S2 (Supporting Information). Note that the background fluorescence intensity is ∼5 counts/10 ms under the excitation power of 0.72 W/cm^2 used for the pure P3HT NPs and ∼15 counts/10 ms with the excitation power of 7.2 W/cm^2 for the composite NPs.

hole-transporting layer of *N*,*N*′-bis(3-methylphenyl)-*N*,*N*′-diphenylbenzidine (TPD, Sigma Aldrich) and the electrode of Au (Cerac, 99.999%) were deposited with thermal evaporation under high vacuum (<10^{-6} Torr) with thicknesses of 50 and 100 nm, respectively. Devices were wired inside the glovebox using silver epoxy (Dynaloy Inc.) and finally encapsulated using UV-curing epoxy (Dymax) and a top protective coverslip to ensure the long-term photostability of the NPs. The F-V/SPS measurement was carried out on a home-built laser confocal scanning microscope (LCSM), which has been described previously elsewhere.[26] Briefly, the fluorescence image was first collected with LCSM under 488 nm excitation when the sample was raster scanned across the focused laser beam (Figure 1). The fluorescence vs time traces for individual NPs were obtained by positioning a chosen NP into the laser beam and recording the fluorescence transients while under continuous laser excitation, with a power of 0.7 W/cm^2 for the pure P3HT NPs and 7 W/cm^2 for the 50 wt % $PC_{60}BM$ blended P3HT NPs. Then, the fluorescence-voltage modulation experiment was conducted by applying a repeatedly triangular waveform of bias voltage, achieved with a programmable wave function generator (Fluke), while acquiring the single particle fluorescence time transient. The data acquisition was in turn synchronized to the applied bias cycles, allowing for the synchronous averaging of the data as a function of time and bias over many cycles.

■ RESULTS AND DISCUSSION

Figure 2 displays the bias-induced fluorescence modulation behavior of both pure P3HT NPs and 50 wt % $PC_{60}BM$ blended P3HT NPs acquired by applying a periodic triangular voltage

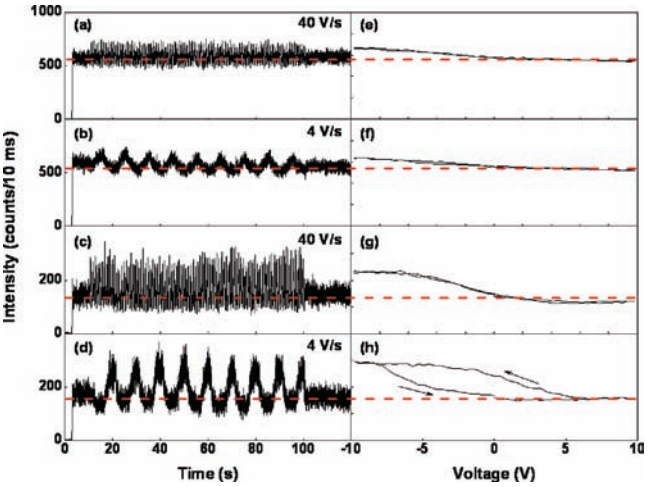

Figure 3. 50 wt % $PC_{60}BM$ blended P3HT NPs fluorescence transients obtained while modulating a triangle bias sequence across the device. Transients in parts a and b displaying low fluorescence recovery under negative bias were acquired from the same nanoparticle under different sweep rates indicated in the figures. Transients in parts c and d showing strong fluorescence recovery were also taken from the same nanoparticle. The right column exhibits corresponding time averaged fluorescence−voltage curves (e−h) derived from the scans in the left column (a−d). The arrows in parts e−h signify the direction of the bias scan.

sequence (Figure 2a) on the hole−injection capacitor device in which these NPs are embedded. During the experiments, two types of modulation behavior were exhibited by each type of NPs. Pure P3HT NPs show either only fluorescence quenching at positive bias (∼84% of NPs) (Figure 2b) or fluorescence quenching at positive bias together with fluorescence recovery at negative bias within a voltage cycle (Figure 2c) (∼16% of NPs). For 50 wt % $PC_{60}BM$ blended P3HT NPs, ∼80% of the NPs only exhibits fluorescence recovery at negative bias, while ∼20% shows fluorescence recovery at negative bias together with fluorescence quenching at positive bias within a voltage cycle, as demonstrated in Figures 2d and e and 3. These observations are discussed below. Averaging these data over a number of bias cycles and replotting as a function of applied bias yields the fluorescence modulation vs bias curves displayed in Figure 2f−i. Minor or no hysteresis is observed for the pure NPs (Figure 2f and g) at the bias scan rates used in this study (4.0 V/s and 40 V/s) and implies rapid hole injection and removal rates. These data indicate fast reaction of mobile holes in the device to the electrical field and only shallow hole trapping (if any) near the TPD/P3HT NP interface.[19,21] In comparison, the data in Figure 2h and i for the 50 wt % $PC_{60}BM$ blended NPs show the occurrence of significant hysteresis, as discussed further below.

The majority (∼84%) of the pure NPs show the modulation behavior depicted in Figure 2b and f. The fluorescence intensity reduces gradually and almost linearly upon applying positive bias to the device, while no detectable intensity enhancement is observed at negative bias. The fluorescence quenching at positive bias, ranging from 5% to 40%, is attributed to a combination of *charge transfer and energy transfer mechanisms* between holes injected in the device at positive bias and singlet excitons that are optically excited in the P3HT NPs.[13,14] The inefficient quenching of fluorescence for the pure NPs can be attributed to the following aspects: (i) hole transfer from TPD to P3HT is isoergic in energetics rather than exoergic;[19,21] and (ii) there is a limited quenching volume of

390 nm^3 for single excitons by holes in conjugated polymers,[10,11] considering the much larger volume of NPs (diameter of ~30 nm in the present case). In addition, the low modulation observed for virtually all P3HT NPs and some of the P3HT/$PC_{60}BM$ NPs (discussed below) could indicate field-induced modulation of the NP fluorescence. Previous investigations have shown electric field-induced conjugated polymer fluorescence quenching by exciton dissociation in the presence of an electric field in metal/polymer/metal devices. While this is a potential mechanism that can account for the absence of hysteresis, fluorescence quenching in both forward and reverse bias would be expected in that case.[27] At negative bias, holes are removed from the device (depletion). The majority (~84%) of the pure NPs do not show obvious fluorescence recovery under these conditions, indicating negligible presence of free charge carriers in these NPs. While it is well-known that if photoinduced free charge carriers ($P3HT^+$ and $P3HT^-$) can be formed in pure P3HT materials, a fluorescence intensity increase would be expected in the reported experiments due to hole (i.e., quencher) removal at negative bias. Only ~16% of the pure NPs exhibit both fluorescence quenching and recovery modulations, as illustrated in Figure 2c and g. This observation indicates the presence of an oxidized state of P3HT (i.e., $P3HT^+$/anion) in these NPs due to either intrinsic free charge carrier formation or photooxidation. Yields of free charge carrier generation for P3HT have been reported to be in the range of 5% to 30% under photoexcitation in the absence of electron acceptors,[28,29] which can explain our observations of recovery at negative bias for a fraction of pure NPs. The occurrence of partially oxidized NPs is expected to be minimal given that care has been taken in eliminating oxygen and water from the device to ensure NP photostability. The instability observed for some NPs is discussed in the Supporting Information (Figure S1).

Considering the 50 wt % $PC_{60}BM$ blended P3HT NPs, the majority (~ 80%) does not exhibit fluorescence quenching at positive bias as shown in Figure 2(d) and Figure 3. With the presence of $PC_{60}BM$, the fluorescence of P3HT in the composite NPs is strongly quenched due to an ultrafast electron transfer process from P3HT to $PC_{60}BM$, which is much faster than the energy transfer process between singlet states and holes.[6] This ultrafast charge transfer process combined with resultant short fluorescence lifetime[28] probably hampers further exciton quenching by injected holes. In addition, the injected hole concentration near the TPD/NP interface might be low due to electrostatic repulsion from photogenerated holes and low bias applied to the device. A fraction (~ 20%) of the blended NPs demonstrate fluorescence quenching of ~10−50% at positive bias in addition to recovery at negative bias (Figure 2e and i). The difference in fluorescence modulation at positive bias observed for the 50 wt % $PC_{60}BM$ blended NPs could be ascribed to heterogeneities of the distribution of components in the NPs e.g. phase separation, slight variations in composition between different NPs, or different local environment of the NPs in the device that may lead to changes in the energetics of interfacial charge and/or energy transfer.

When negative bias is applied to the device, nearly all the 50 wt % $PC_{60}BM$ blended P3HT NPs show obvious fluorescence recovery ranging from 10% up to 100% (Figure 3a−d). This observation provides clear evidence of the presence of free charge carriers ($P3HT^+$ and $PC_{60}BM^-$) due to photoinduced charge transfer from P3HT to $PC_{60}BM$ in the composite NPs. In the current case, P3HT is oxidized to its cation ($P3HT^+$, quenched state) via charge transfer to $PC_{60}BM$ under photoexcitation. The $P3HT^+$ cation is reduced to its emissive state (under excitation) by hole removal at negative bias. The observation of fluorescence recovery for the oxidized P3HT when applying negative bias is to some extent in analogy to that found for photooxidized MEH-PPV single molecules, for which the photochemical species are suspected to be MEH-PPV^+/O_2^- (OH^-).[13] However, specific to the 50 wt % $PC_{60}BM$ blended P3HT NPs, additional trends in the bias-induced fluorescence modulation are observed at negative bias. First, in the negative bias region, the photooxidized MEH-PPV single molecule fluorescence recovery shows a pronounced plateau, caused by a rapid and reversible single electron transfer process in a two-level system (oxidized and reduced species).[13,14] In comparison, the composite NP data display a gradual modulation behavior as a function of applied bias, especially for NPs exhibiting small fractions of fluorescence recovery with respect to the baseline (zero bias) fluorescence; see Figure 3a, b, e, and f. This gradual modulation behavior as opposed to an ON/OFF switching between two discrete states as found for single molecules or NPs[13,14] can be explained by the presence of multiple P3HT molecules in the NPs that exhibit charge transfer to $PC_{60}BM$ in the NPs or energy/charge transfer across the TPD/NP interface at different times and with different rates. Second, as shown in Figure 3c, d, g, and h), for the blended NPs, *stronger hysteresis at slower sweep rates* as opposed to faster sweep rates (as observed for MEH-PPV single molecules and NPs[13,14,19]) is observed, and this hysteresis effect is found mostly for NPs showing strong fluorescence intensity recovery at negative bias. Thus, for the 50 wt % $PC_{60}BM$ blended P3HT NPs, the observed hysteresis is strongly related to the modulation depth. Composite NPs (~27%) showing weak recoveries, as portrayed in Figure 3a and b, do not show a significant hysteresis for the sweep rates used (i.e., 40 V/s and 4.0 V/s in Figure 3e and f, respectively), implying a rapid hole removal and retrieval process, probably due to only shallow charge traps at the TPD/NP interface or an absence of charge trapping at the NP/dielectric interface *due to a low population of free charge carriers being generated in these specific NPs.*[19,21,30] The lower population of free charge carriers in these NPs may be due to compartmentalization (phase separation) of P3HT and $PC_{60}BM$ in the NPs or low presence of $PC_{60}BM$ in these NPs. In addition, there may be poor contact of the NPs with the TPD/Au electrode. However, the 50 wt % blended NPs showing strong modulation behavior (~53%), i.e. large fraction of fluorescence recovery with respect to the baseline (zero bias) fluorescence when studied under a (low) sweep rate of 4.0 V/s, exhibit a large hysteresis, as shown in Figure 3d and h. Specially, as shown in Figure 3c and d, a large anticlockwise hysteresis was observed at a slow sweep rate (4.0 V/s). This observation is quite distinct from that found for previously investigated photooxidized MEH-PPV single molecules or NPs, in which higher sweep rates typically yield larger clockwise hysteresis due to slow interfacial kinetics; that is, the oxidation/reduction process is cycled too rapidly to be able to reach equilibrium.[14,19] Although these two systems seem analogous in terms of photochemically formed species, i.e., $P3HT^+$/$PC_{60}BM^-$ for the composite NPs under photoexcitation in this work and MEH-PPV^+/anions in photooxidized MEH-PPV single molecules,[13,14] significant differences should be noted. In the composite NPs, emissive excitons coexist with a large amount of free charges, including $P3HT^+$; $PC_{60}BM^-$, originating from charge transfer from P3HT to $PC_{60}BM$; and $P3HT^-$, originating from direct P3HT exciton dissociation,[28,31] all of which impose significant effects on interfacial charge transfer processes and trapping. Furthermore, Drori et al. have shown that a ground state

charge transfer complex (GSCTC) is formed inside the optical gap of P3HT and $PC_{60}BM$, where the resulting charge transfer excitons can generate polarons that can become trapped at the polymer/fullerene interfaces.[32] This mechanism may have a contribution in the observed modulation behaviors and variation in hysteresis observed for the 50 wt % $PC_{60}BM$ blended P3HT NPs. The contribution is however difficult to quantify, since it strongly depends on the intrachain conjugated polymer morphology.[33] The specifics of these processes will now be further discussed by means of the data and schematics presented in Figure 4.

Starting from 0 V and sweeping to +10 V, holes injected into the TPD layer are expected to be accumulated near the TPD/dielectric and TPD/NP interfaces at sufficiently high positive bias voltage. Hole accumulation and trapping most likely occur at these interfaces; albeit, the traps are shallow (Figure 4b).[19,21,30] Several studies have shown that fullerene anions can act as effective deep hole traps.[34] It is therefore likely that a fraction of the population of photogenerated holes and/or electronically injected holes remain trapped by proximal $PC_{60}BM$ anions. When cycling back from +10 to 0 V, photogenerated holes in the composite NPs and holes in TPD are gradually removed with decreasing positive bias, bringing the device toward hole depletion. Holes in shallow traps are quickly removed as well (Figure 4c). As a result, the population of P3HT cations is gradually reduced to neutral P3HT molecules, which can be observed by a fluorescence increase with respect to the baseline fluorescence as the bias evolves to negative voltages. Continuing to reverse bias from 0 to −10 V, more and more photogenerated holes are removed from the NP until the fluorescence recovery reaches a plateau when the applied bias exceeds −5 V. At that point, the device appears as being fully depleted from photogenerated and previously injected holes. During this process, there is still photogeneration of holes and electrons, but holes are quickly removed from the device. Thus, an excess of electrons is built up near the NPs and NP/dielectric interfaces (Figure 4d). Previous literature reports have extensively documented that electrons can be deeply trapped at organic/dielectric interfaces, or even in the bulk of the dielectric, and that $PC_{60}BM$ is a deep electron trap as well.[23,35] In these cases, anticlockwise hysteresis in capacitance−voltage data was typically observed.[23,36] In addition, when comparing the forward sweep curve obtained at 4.0 V/s, particularly from −10 to 0 V (forward sweep), with the corresponding fast scan curves obtained at 40 V/s, a negative shift is evident for the slow scan curve in the data reported herein. Similar observations have been reported previously for capacitance−voltage measurements on polymer−dielectric two-terminal and three-terminal devices.[24,37] Several reports have also been made where capacitance−voltage measurements were completed on P3HT and P3HT/$PC_{60}BM$ two-terminal and three-terminal devices under illumination.[22−24] Strong hysteresis was observed in all of the reports and was attributed to a build-up of free carriers due to photoinduced charge transfer from P3HT to $PC_{60}BM$ or spontaneous exciton dissociation in the absence of $PC_{60}BM$, that results in trapping of electrons at the organic/dielectric interface. This assignment was supported particularly well in the report by Lancaster et al., where a control experiment was also completed while optically exciting the device outside of the P3HT absorption band. In that case, no accumulation and trapping of electrons was observed due to the low exciton generation rate near the organic/dielectric interface.[24] On the basis of these literature reports, it is thus reasonable to assign the observed anticlockwise hysteresis at lower bias sweep rates for the single composite P3HT/$PC_{60}BM$ NPs to the trapping of photogenerated free

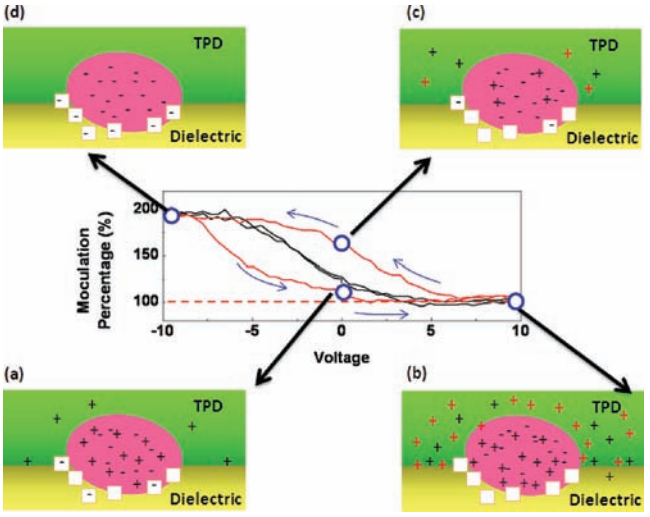

Figure 4. (middle panel) Data plot displaying time averaged fluorescence intensity modulation percentage vs voltage curves collected for the same 50 wt % $PC_{60}BM$ blended P3HT nanoparticle at sweep rates of 4.0 V/s (black) and 40 V/s (red). The red dashed line indicates the baseline fluorescence modulation percentage (at zero bias). The blue arrows show the direction of the voltage scan (starting from 0 V). The four circles on the black curve indicate the conditions that are being represented by the cartoons. The pink ellipsoid represents a nanoparticle, and the white squares indicate electron trap sites. The red and black "+" symbols represent bias injected holes and photogenerated holes, respectively, while the black "−" symbols represent photogenerated electrons.

electrons at the P3HT/dielectric interface and/or on $PC_{60}BM$.[38] The absence of hysteresis at higher sweep rates is attributed to the absence of deeply trapped electrons, where the fast bias sweep itself prevents electrons from becoming deeply trapped, presumably through quick recombination with injected and photogenerated holes. Palacios et al. have made comparable observations for poly(9,9-di-*n*-octylfluorene-alt-benzothiadiazole) (F8BT) NPs embedded in an electrochemical cell.[11]

Detrapping and removal of electrons is expected to occur during the forward sweep (from −10 to +10 V). During the forward sweep, holes start to accumulate in the polymer NPs (as evidenced by the decreasing fluorescence signal) and can recombine with trapped electrons (Figure 4a). In addition, the electric field in the device during the forward sweep will help to detrap electrons. However, electrons are not likely to be injected back into the NPs or TPD layers, so the removal of electrons by recombination with holes is limited by the rate at which photogenerated and injected holes reach the organic/dielectric interface.[23,37] As shown in the middle panel of Figure 4, the reverse sweep (+10 to −10 V) under slow scan conditions is shifted to positive bias compared to the faster scan experiment, probably because of hole trapping by $PC_{60}BM$ anions in the composite NPs given that this effect was not observed for pure NPs.[34]

In summary, the hysteretic data observed for single composite P3HT/$PC_{60}BM$ NPs under illumination in the hole-only capacitor devices discussed above clearly indicate electrically bistable behavior due to electron trapping at the organic/dielectric interfaces and hole trapping by fullerene anions in composite P3HT/$PC_{60}BM$ NPs under photoexcitation. These experimental results are promising for future applications of donor−acceptor composite NPs in *photocontrolled memory devices,*

metal−insulator−semiconductor (MOS) imaging devices, and *photoresponsive OFETs,* with the potential for nanoscale or single NP device elements.

CONCLUSION

Memory functions via optical programming and electrical erasing have been reported for bulk P3HT/PC_{60}BM and P3HT/CdSe based devices and attributed to electron trapping−detrapping near the organic/dielectric interface and on the electron acceptors present in these blended materials.[22,23] In the present paper, fluorescence-voltage/single particle spectroscopy (F-V/SPS) was employed to study exciton−hole polaron interactions and interfacial charge transfer processes for *individual* pure P3HT nanoparticles (NPs) and composite P3HT/PC_{60}BM NPs in functioning hole-injection devices. F-V/SPS data collected for individual NPs reveal an apparent hysteresis in the data for composite P3HT/PC_{60}BM NPs that is attributed to the deep trapping of photogenerated free electrons at the organic/dielectric interface and hole trapping by fullerene anions in composite P3HT/PC_{60}BM NPs under photoexcitation. This investigation of charge trapping based on single NPs opens the door for novel approaches to understanding the charge-storage mechanism on the nanometer scale and future applications of composite conjugated polymer NPs in nanoscale memory and photoresponsive devices such as light activated switches and light induced amplifiers.

ASSOCIATED CONTENT

Supporting Information. Data on optoelectronic instability of nanoparticles: fluorescence transients and F-V modulations at a bias sweep rate of 40 V/s applied to the device. This material is available free of charge via the Internet at http://pubs.acs.org.

AUTHOR INFORMATION

Corresponding Author
andre@ucf.edu

ACKNOWLEDGMENT

The authors wish to thank the National Science Foundation (NSF) for financial support of this work through a CAREER award (CBET-0746210) and through award ECCS-0801924.

REFERENCES

(1) Sariciftci, N. S.; Smilowitz, L.; Heeger, A. J.; Wudl, F. *Science* **1992**, *258*, 1474.

(2) (a) Thompson, B. C.; Frechet, J. M. J. *Angew. Chem., Int. Ed.* **2008**, *47*, 58. (b) Liang, Y. Y.; Xu, Z.; Xia, J. B.; Tsai, S. T.; Wu, Y.; Li, G.; Ray, C.; Yu, L. P. *Adv. Mater.* **2010**, *22*, E135. (c) Chen, H.-Y.; Hou, J.; Zhang, S.; Liang, Y.; Yang, G.; Yang, Y.; Yu, L.; Wu, Y.; Li, G. *Nat. Photonics* **2009**, *3*, 649.

(3) (a) Zaumseil, J.; Sirringhaus, H. *Chem. Rev.* **2007**, *107*, 1296. Meijer, E. J.; De Leeuw, D. M.; Setayesh, S.; Van Veenendaal, E.; Huisman, B. H.; Blom, P. W. M.; Hummelen, J. C.; Scherf, U.; Klapwijk, T. M. *Nat. Mater.* **2003**, *2*, 678. (b) Marjanovic, N.; Singh, T. B.; Dennler, G.; Gunes, S.; Neugebauer, H.; Sariciftci, N. S.; Schwodiauer, R.; Bauer, S. *Org. Electron.* **2006**, *7*, 188.

(4) Clarke, T. M.; Durrant, J. R. *Chem. Rev.* **2010**, *110*, 6736.

(5) Bredas, J. L.; Norton, J. E.; Cornil, J.; Coropceanu, V. *Acc. Chem. Res.* **2009**, *42*, 1691.

(6) Ferguson, A. J.; Kopidakis, N.; Shaheen, S. E.; Rumbles, G. *J. Phys. Chem. C* **2008**, *112*, 9865.

(7) Liu, C. Y.; Chen, S. A. *Macromol. Rapid Commun.* **2007**, *28*, 1743.

(8) (a) Byers, J. C.; Ballantyne, S.; Rodionov, K.; Mann, A.; Semenikhin, O. A. *ACS Appl. Mater. Interfaces* **2011**, *3*, 392. (b) Groves, C.; Blakesley, J. C.; Greenham, N. C. *Nano Lett.* **2010**, *10*, 1063.

(9) (a) Barbara, P. F.; Gesquiere, A. J.; Park, S. J.; Lee, Y. J. *Acc. Chem. Res.* **2005**, *38*, 602. (b) Lupton, J. M. *Adv. Mater.* **2010**, *22*, 1689. (c) Vacha, M.; Habuchi, S. *NPG Asia Mater.* **2010**, *2*, 134. (d) Mirzov, O.; Scheblykin, I. G. *Phys. Chem. Chem. Phys.* **2006**, *8*, 5569. (e) Chang, W.-S.; Link, S.; Yethiraj, A.; Barbara, P. F. *J. Phys. Chem. B* **2008**, *112*, 448. (f) Sherwood, G. A.; Cheng, R.; Smith, T. M.; Werner, J. H.; Shreve, A. P.; Peteanu, L. A.; Wildeman, J. *J. Phys. Chem. C* **2009**, *113*, 18851. (g) Karam, P.; Ngo, A. T.; Rouiller, I.; Cosa, G. *Proc. Natl. Acad. Sci. U. S. A.* **2010**, *107*, 17480. (h) Tcherniak, A.; Ha, J. W.; Dominguez-Medina, S.; Slaughter, L. S.; Link, S. *Nano Lett.* **2010**, *10*, 1398. (i) English, D. S.; Harbron, E. J.; Barbara, P. F. *J. Chem. Phys.* **2001**, *114*, 10479. (j) Patra, D. *Appl. Spectrosc. Rev.* **2008**, *43*, 389. (k) Reznik, C.; Berg, R.; Foster, E.; Advincula, R.; Landes, C. F. *J. Phys. Chem. Lett.* **2011**, *2*, 592.

(10) Yu, J.; Song, N. W.; McNeill, J. D.; Barbara, P. F. *Isr. J. Chem.* **2004**, *44*, 127.

(11) Palacios, R. E.; Fan, F. R. F.; Grey, J. K.; Suk, J.; Bard, A. J.; Barbara, P. F. *Nat. Mater.* **2007**, *6*, 680.

(12) Gesquiere, A. J.; Park, S. J.; Barbara, P. F. *J. Am. Chem. Soc.* **2005**, *127*, 9556.

(13) Park, S. J.; Gesquiere, A. J.; Yu, J.; Barbara, P. F. *J. Am. Chem. Soc.* **2004**, *126*, 4116.

(14) Gesquiere, A. J.; Park, S. J.; Barbara, P. F. *J. Phys. Chem. B* **2004**, *108*, 10301.

(15) Gesquiere, A. J.; Lee, Y. J.; Yu, J.; Barbara, P. F. *J. Phys. Chem. B* **2005**, *109*, 12366. Palacios, R. E.; Barbara, P. F. *J. Fluoresc.* **2007**, *17*, 749.

(16) Bolinger, J. C.; Fradkin, L.; Lee, K. J.; Palacios, R. E.; Barbara, P. F. *Proc. Natl. Acad. Sci. U. S. A.* **2009**, *106*, 1342.

(17) Lee, Y. J.; Park, S. J.; Gesquiere, A. J.; Barbara, P. F. *Appl. Phys. Lett.* **2005**, *87*, 051906.

(18) Yu, J.; Lammi, R.; Gesquiere, A. J.; Barbara, P. F. *J. Phys. Chem. B* **2005**, *109*, 10025.

(19) Palacios, R. E.; Lee, K. J.; Rival, A.; Adachi, T.; Bolinger, J. C.; Fradkin, L.; Barbara, P. F. *Chem. Phys.* **2009**, *357*, 21.

(20) Fradkin, L.; Palacios, R. E.; Bolinger, J. C.; Lee, K. J.; Lackowski, W. M.; Barbara, P. F. *J. Phys. Chem. A* **2009**, *113*, 4739.

(21) Bolinger, J.; Lee, K. J.; Palacios, R. E.; Barbara, P. F. *J. Phys. Chem. C* **2008**, *112*, 18608.

(22) Chen, C. C.; Chiu, M. Y.; Sheu, J. T.; Wei, K. H. *Appl. Phys. Lett.* **2008**, *92*, 143105.

(23) Mohamad, K. A.; Goto, K.; Uesugi, K.; Fukuda, H. *Jpn. J. Appl. Phys.* **2010**, *49*, 06GG09.

(24) Lancaster, J.; Taylor, D. M.; Sayers, P.; Gomes, H. L. *Appl. Phys. Lett.* **2007**, *90*, 103513.

(25) Taylor, D. M.; Drysdale, J. A.; Torres, I.; Fernandez, O. *Appl. Phys. Lett.* **2006**, *89*, 183512.

(26) Hu, Z. J.; Tenery, D.; Bonner, M. S.; Gesquiere, A. J. *J. Lumin.* **2010**, *130*, 771. Tenery, D.; Worden, J. G.; Hu, Z. J.; Gesquiere, A. J. *J. Lumin.* **2009**, *129*, 423.

(27) (a) Moscatelli, A.; Livingston, K.; So, W. Y.; Lee, S. J.; Scherf, U.; Wildeman, J.; Peteanu, L. A. *J. Phys. Chem. B* **2010**, *114*, 14430. (b) Singh, V.; Thakur, A. K.; Pandey, S. S.; Takashima, W.; Kaneto, K. *Synth. Met.* **2008**, *158*, 283. (c) Schindler, F.; Lupton, J. M.; Muller, J.; Feldmann, J.; Scherf, U. *Nat. Mater.* **2006**, *5*, 141. (d) Scheblykin, I.; Zoriniants, G.; Hofkens, J.; De Feyter, S.; Van der Auweraer, M.; De Schryver, F. C. *ChemPhysChem* **2003**, *4*, 260. (e) Adams, D. M.; Kerimo, J.; Liu, C. Y.; Bard, A. J.; Barbara, P. F. *J. Phys. Chem. B* **2000**, *104*, 6728. (f) Arkhipov, V. I.; Bassler, H.; Deussen, M.; Gobel, E. O.; Kersting, R.; Kurz, H.; Lemmer, U.; Mahrt, R. F. *Phys. Rev. B* **1995**, *52*, 4932. (g) Arkhipov, V. I.; Bassler, H.; Deussen, M.; Gobel, E. O.; Lemmer, U.; Mahrt, R. F. *J. Non-cryst. Solids* **1996**, *200*, 661. (h) Deussen, M.; Bolivar, P. H.; Wegmann, G.; Kurz, H.; Bassler, H. *Chem. Phys.* **1996**,

207, 147. (i) Deussen, M.; Scheidler, M.; Bassler, H. *Synth. Met.* **1995**, *73*, 123.

(28) Piris, J.; Dykstra, T. E.; Bakulin, A. A.; van Loosdrecht, P. H. M.; Knulst, W.; Trinh, M. T.; Schins, J. M.; Siebbeles, L. D. A. *J. Phys. Chem. C* **2009**, *113*, 14500.

(29) (a) Dicker, G.; de Haas, M. P.; Siebbeles, L. D. A.; Warman, J. M. *Phys. Rev. B* **2004**, *70*, 045203. (b) Sheng, C. X.; Tong, M.; Singh, S.; Vardeny, Z. V. *Phys. Rev. B* **2007**, *75*, 085206.

(30) Karg, S.; Steiger, J.; von Seggern, H. *Synth. Met.* **2000**, *111*, 277.

(31) Grzegorczyk, W. J.; Savenije, T. J.; Dykstra, T. E.; Piris, J.; Schins, J. M.; Siebbeles, L. D. A. *J. Phys. Chem. C* **2010**, *114*, 5182.

(32) Drori, T.; Holt, J.; Vardeny, Z. V. *Phys. Rev. B* **2010**, 82.

(33) Hallermann, M.; Da Como, E.; Feldmann, J.; Izquierdo, M.; Filippone, S.; Martin, N.; Juechter, S.; von Hauff, E. *Appl. Phys. Lett.* **2010**, 97.

(34) (a) Youn, J. H.; Lee, Y. I.; Moon, H. T.; Ryu, M. S.; Kim, J.; Jang, J. *Curr. Appl. Phys.* **2010**, *10*, S525. (b) Nam, C. Y.; Su, D.; Black, C. T. *Adv. Funct. Mater.* **2009**, *19*, 3552. (c) Grunnet-Jepsen, A.; Wright, D.; Smith, B.; Bratcher, M. S.; DeClue, M. S.; Siegel, J. S.; Moerner, W. E. *Chem. Phys. Lett.* **1998**, *291*, 553.

(35) Kusunoki, T.; Nakayama, K.; Pu, Y. J.; Kido, J. *Mol. Cryst. Liq. Cryst.* **2009**, *504*, 124.

(36) (a) Liu, J. Q.; Yin, Z. Y.; Cao, X. H.; Zhao, F.; Lin, A. P.; Xie, L. H.; Fan, Q. L.; Boey, F.; Zhang, H.; Huang, W. *ACS Nano* **2010**, *4*, 3987. (b) Singh, B.; Marjanovic, N.; Sariciftci, N. S.; Schwodiauer, R.; Bauer, S. *IEEE Trans. Dielectr. Electr. Insul.* **2006**, *13*, 1082. (c) Chu, C. W.; Ouyang, J.; Tseng, H. H.; Yang, Y. *Adv. Mater.* **2005**, *17*, 1440.

(37) William, S.; Mabrook, M. F.; Taylor, D. M. *Appl. Phys. Lett.* **2009**, *95*, 093309.

(38) The trapped electron density can be roughly estimated, as discussed in refs 24 and 39, from the negative voltage shift of the forward sweep curve (i.e., from −10 to 10 V) when comparing the slow sweep and fast sweep data and the relation $Q = C_i\Delta V/A$, where C_i is the insulator capacitance, ΔV is the shift in the voltage, which is about 2.5 V (Figure 4), and A is the device area of 0.066 cm^2. C_i is calculated to be 0.5 nF via $C_i = \varepsilon_r\varepsilon_0 A/d$, where $\varepsilon_r = 3$, and the dielectric layer thickness d = 350 nm. From this approximation the density of trapped electrons is found to be $1.2 \times 10^{11}/cm^2$.

(39) Yun, M.; Ravindran, R.; Hossain, M.; Gangopadhyay, S.; Scherf, U.; Bunnagel, T.; Galbrecht, F.; Arif, M.; Guha, S. *Appl. Phys. Lett.* **2006**, *89* (1), 013506.